RELAXATION AND APPROXIMATE FACTORIZATION METHODS FOR THE UNSTEADY FULL POTENTIAL EQUATION

Vijaya Shankar*, Hiroshi Ide**, and Joseph Gorski†
Rockwell International Science Center
Thousand Oaks, California 91360

Abstract

The unsteady form of the full potential equation is solved in conservation form using implicit methods based on approximate factorization and relaxation schemes. A local time linearization for density is introduced to enable solution to the equation in terms of ϕ, the velocity potential. A novel flux biasing technique is applied to generate proper forms of the artificial viscosity to treat hyperbolic regions with shocks and sonic lines present. The wake is properly modeled by accounting not only for jumps in ϕ, but also for jumps in higher derivatives of ϕ, obtained from requirements of density continuity. The far field is modeled using the Riemann invariants to simulate nonreflecting boundary conditions. Results are presented for flows over airfoils, cylinders, and spheres. Comparisons are made with available Euler and full potential results.

I. Introduction

Nonlinear aerodynamic prediction methods based on the steady form of the full potential equation are used regularly for treating transonic[1,2] and supersonic[3-6] flows over realistic wing–body configurations. Numerical algorithms to compute the unsteady form of the full potential equation are still in a developmental stage, and several researchers[7-11] have recently made significant progress in this area. There are several issues involved in the construction of a robust and efficient numerical algorithm for the unsteady full potential equation. They are: 1) proper treatment of boundary conditions in a nonorthogonal grid system, 2) correct formulation for the production of artificial viscosity to capture sharp shocks, 3) proper time linearization concepts, 4) unsteady wake treatment, and 5) nonreflecting outer boundary conditions.

The objective of the present paper is to present a numerical treatment of the unsteady full potential equation that properly takes into account the importance of the above listed items. The paper discusses a local time linearization procedure for treating the time derivative term, a flux biasing concept based on sonic conditions (instead of the usual density biasing procedures) for the treatment of spatial derivative terms, split boundary condition procedures consistent with approximate factorization schemes, unsteady wake models with proper jumps in ϕ and higher derivatives of ϕ taken into account from density relationships, and nonreflecting unsteady far field procedures based on Riemann invariants derived from the characteristic theory.

Use of unsteady methods has application not only to unsteady problems, but also to time asymptotic steady state solutions. If the unsteady method is constructed properly (robust and efficient), then it can even be made to generate steady state solutions faster than methods based on the steady form of the equation. Also, in the unsteady method, since the time direction is always present, the hyperbolicity of the unsteady full potential equation will allow one to obtain solutions to problems across the Mach number range (subsonic, transonic, and supersonic), whether steady or unsteady. The unsteady method of this paper, when combined with the steady marching method of Refs. 4–6, provides a complete treatment of the full potential equation.

Results are presented for flows over cylinders, spheres, and airfoils at various Mach numbers, and some comparisons are made with Euler solutions. Use of the split boundary condition technique, combined with the flux biasing concepts[12,13], has produced a very robust method which, even for a difficult case with a fishtail shock at the trailing edge of an airfoil, did not require any user-specified "constants", such as the ones discussed in Ref. 2.

The paper also presents the results from a "hybrid" calculation, wherein the spherical blunt body solution from the unsteady code has been effectively used to provide the initial data plane for a supersonic marching calculation performed over the Shuttle Orbiter geometry.

II. Formulation

The two–dimensional/axisymmetric unsteady full potential equation written in a body–fitted coordinate system represented by $\tau = t$, $\zeta = \zeta(x,y,t)$ and $\eta = \eta(x,y,t)$ takes the form

$$\left(\frac{\rho}{J}\right)_\tau + \left(\rho\frac{U}{J}\right)_\zeta + \left(\rho\frac{V}{J}\right)_\eta + S\rho\frac{v}{yJ} = 0 \qquad (1)$$

where

$S = 0$ for two dimensions, $= 1$ for axisymmetric

$$\rho = \text{density} = \left[1 - \tfrac{\gamma-1}{2}M_\infty^2\,(2\phi_\tau + \bar{U}\phi_\zeta + \bar{V}\phi_\eta - 1\right]^{1/(\gamma-1)}$$

$$U = \zeta_t + a_{11}\phi_\zeta + a_{12}\phi_\eta;\ \bar{U} = U + \zeta_t$$

$$V = \eta_t + a_{12}\phi_\zeta + a_{22}\phi_\eta;\ \bar{V} = V + \eta_t$$

$$a_{11} = \zeta_x^2 + \zeta_y^2;\ a_{12} = \zeta_x\eta_x + \zeta_y\eta_y$$

$$a_{22} = \eta_x^2 + \eta_y^2$$

$$J = \text{Jacobian} = \zeta_x\eta_y - \zeta_y\eta_y$$

The density ρ and the fluxes ρU and ρV are complicated nonlinear functions of ϕ, the velocity potential.

*Manager, Computational Fluid Dynamics Group

**Member Technical Staff, Aircraft Operations Div.

†Senior Technical Associate

Hence, to solve for ϕ from Eq. (1) will require a local linearization.

Let 'n' be the running index in the time direction, 'k' in the ζ direction, and 'j' in the η direction leading out of the surface. The objective is to solve Eq. (1) for $\phi_{j,k}^{n+1}$ at the current time plane, knowing the information at n, $n-1$, $n-2$, $\cdots$ planes.

A. Treatment of $\frac{\partial}{\partial\tau}\left(\frac{\rho}{J}\right)$ in Eq. (1)

$$\frac{\partial}{\partial\tau}\left(\frac{\rho}{J}\right)^{n+1} =$$

$$\frac{(a_1-\theta b_1)\left\{\left(\frac{\rho}{J}\right)^{n+1}-\left(\frac{\rho}{J}\right)^{n}\right\}-\theta b_1\left\{\left(\frac{\rho}{J}\right)^{n}-\left(\frac{\rho}{J}\right)^{n-1}\right\}}{a_1\Delta\tau_1-\theta b_1\left(\Delta\tau_1+\Delta\tau_2\right)} \tag{2}$$

where

$a_1 = (\Delta\tau_1+\Delta\tau_2)^2$

$b_1 = \Delta\tau_1^2$

$\theta = 0$ for first order time accuracy

$\theta = 1$ for second order accuracy

$\Delta\tau_1 = \tau^{n+1}-\tau^n$

$\Delta\tau_2 = \tau^n-\tau^{n-1}$

In order to write Eq. 2 in terms of ϕ^{n+1}, a local time linearization procedure is introduced.

$$\rho^{n+1} \doteq \rho^n + \left(\frac{\partial\rho}{\partial\phi}\right)^n \Delta\phi + \cdots \tag{3}$$

where $\Delta\phi = \left(\phi^{n+1}-\phi^n\right)$. The term $\left(\frac{\partial\rho}{\partial\phi}\right)$ is a differential operator given by

$$\left(\frac{\partial\rho}{\partial\phi}\right)^n = -\frac{\rho^n}{a^2}\left(\frac{\partial}{\partial\tau}+U^n\frac{\partial}{\partial\zeta}+V^n\frac{\partial}{\partial\eta}\right) \tag{4}$$

where 'a' is the local speed of sound.

Combining Eqs. (3) and (4), the nonlinear density function in terms of ϕ has been linearized, and the coefficients multiplying $\Delta\phi$ are evaluated at the known previous time level. To maintain conservation form, both ρ^{n+1} and ρ^n appearing in the first term of Eq. (2) are linearized according to Eq. (3).

B. Treatment of $\frac{\partial}{\partial\zeta}\left(\rho\frac{U}{J}\right)$

$$\left(\rho\frac{U}{J}\right)_\zeta^{n+1} = \overleftarrow{\frac{\partial}{\partial\zeta}}\left(\frac{\tilde\rho_{j,k+1/2}U_{j,k+1/2}^{n+1}}{J_{j,k+1/2}}\right)$$

$$= \overleftarrow{\frac{\partial}{\partial\zeta}}\left\{\frac{\tilde\rho}{J}\left(a_{11}\left\{\Delta\phi+\phi^n\right\}_\zeta + a_{12}\left\{\Delta\phi+\phi^n\right\}_\eta\right)\right\}_{j,k+1/2} \tag{5}$$

where $\rho_{j,k+1/2}^{n+1}$ appearing in the spatial derivative term has been linearized to $\tilde\rho_{j,k+1/2}$. The symbol $\tilde{}$ appearing over ρ denotes that the density has been modified to produce the necessary artificial viscosity. The modified density is obtained from a flux biasing concept to be described later in this paper. For a genuine unsteady problem (where a time asymptotic steady state does not exist), initially, $\tilde\rho$ is set to $\tilde\rho^n$ and then subsequently iterated to convergence by setting $\tilde\rho$ to the pre–time plane. For problems where the steady state exists and is of interest (steady transonic flow over airfoils or blunt objects), $\tilde\rho$ is always set to $\tilde\rho^n$ and requires no internal iterations at the $n+1$ plane.

The only unknown in Eq. (5) is $\Delta\phi$.

C. Treatment of $\frac{\partial}{\partial\eta}\left(\rho\frac{V}{J}\right)$

$$\left(\rho\frac{V}{J}\right)_\eta^{n+1} \doteq \overleftarrow{\frac{\partial}{\partial\eta}}\left(\tilde\rho\frac{V^{n+1}}{J^{n+1}}\right)_{j+1/2,k}$$

$$= \overleftarrow{\frac{\partial}{\partial\eta}}\left\{\frac{\tilde\rho}{J^{n+1}}\left(a_{12}\left\{\Delta\phi+\phi^n\right\}_\zeta + a_{22}\left\{\Delta\phi+\phi^n\right\}_\eta\right)\right\}_{j+1/2,k} \tag{6}$$

Similarly, $\tilde\rho_{j+1/2,k}$ is a modified density based on flux biasing.

D. Biasing Procedure

The spatial derivative terms given by Eqs. (5) and (6) are central differenced expressions about the node point (j,k) and are symmetric operators. For shocked flows and for treatment of hyperbolic regions, these operators are desymmetrized by introducing the biased value of density in the upwind direction. This will create the necessary artificial viscosity to form shocks and exclude the expansion shock. The biased value of density $\tilde\rho$ can be obtained in several ways. Some of them are presented here.

a) Density Biasing[2] (in the ζ–direction)

$$\tilde\rho_{k+1/2} = \rho_{k+1/2} \mp \nu\Delta\zeta\left(\overleftrightarrow{\frac{\partial\rho}{\partial\zeta}}\right)_{k+1/2},$$

$$\nu = \max\left(0, 1-\frac{1}{M^2}\right)_{k+1/2} \tag{7}$$

where M is the local Mach number. For $U>0$, the $-$ sign and backward differencing ($\leftarrow$) is used in Eq. (7), while for $U<0$, the $+$ sign and ($\rightarrow$) operator is used.

b) Directional Flux Biasing

$$\tilde\rho = \frac{1}{q}\left\{\rho q \mp \Delta\zeta\overleftrightarrow{\frac{\partial}{\partial\zeta}}(\rho q)^-\right\} \tag{8}$$

c) Streamwise Flux Biasing

$$\tilde{\rho} = \frac{1}{q}\left\{\rho q \mp \Delta S \overleftrightarrow{\frac{\partial}{\partial S}}(\rho q)^-\right\} \tag{9}$$

where S is the local streamwise direction. Equation (9) can be rearranged as

$$\tilde{\rho} = \frac{1}{q}\left[\rho q \mp \left\{\frac{U}{Q}\Delta\zeta \overleftrightarrow{\frac{\partial}{\partial\zeta}} + \frac{V}{Q}\Delta\eta \overleftrightarrow{\frac{\partial}{\partial\eta}}\right\}(\rho q)^-\right] \tag{10}$$

where $Q = \sqrt{U^2 + V^2}$.

In Eqs. (8) and (10), the term $(\rho q)^-$ is defined to be

$$\begin{aligned}(\rho q)^- &= \rho q - \rho^* q^* \qquad \text{if } q > q^* \\ &= 0 \qquad\qquad\quad \text{if } q \le q^*\end{aligned} \tag{11}$$

The quantities $\rho^* q^*$, ρ^*, and q^* represent sonic values of the flux, density, and total velocity, respectively. These sonic conditions are given by (using the density and speed of sound relationships)

$$(q^*)^2 = \frac{1 + \frac{(\gamma-1)}{2}M_\infty^2\,(1 - 2\phi_\tau - \zeta_t\phi_\zeta - \eta_t\phi_\eta)}{\frac{\gamma+1}{2}M_\infty^2} \tag{12}$$

$$\rho^* = (q^* M_\infty)^{2/(\gamma-1)}.$$

Note that for steady flows, the sonic conditions ρ^* and q^* are only a function of the freestream Mach number, and for a given flow they are constants. For unsteady flows, ρ^* and q^* need to be computed everywhere due to the presence of ϕ_τ and other unsteady terms in Eq. (12).

The density biasing based on flux, Eq. (10), is more accurate than the one presented in Eq. (7), since it is based on sonic reference conditions. To illustrate the flux biasing procedure for various situations, Eq. (8) is considered.

1) Subsonic Flow ($q < q^*$ at $(j, k+1/2)$ and $(j, k-1/2)$) for $U > 0$, the modified density in Eq. (8) becomes

$$\begin{aligned}\tilde{\rho}_{j,k+1/2} = \frac{1}{q_{j,k+1/2}}\Big\{&(\rho q)_{j,k+1/2} \\ &- \left[(\rho q)^-_{j,k+1/2} - (\rho q)^-_{j,k-1/2}\right]\Big\}\end{aligned} \tag{13}$$

$= \rho_{j,k+1/2}$ (since $(\rho q)^-$ at $(j, k+1/2)$ and $(j, k-1/2)$ is zero, according to Eq. (11).

2) Supersonic Flow ($q > q^*$ at $(j, k+1/2)$ and $(j, k-1/2)$) for $U > 0$,

$$\begin{aligned}\tilde{\rho}_{j,k+1/2} &= \frac{1}{q_{j,k+1/2}}\{(\rho q)_{j,k+1/2} \\ &-[(\rho q - \rho^* q^*)_{j,k+1/2} - (\rho q - \rho^* q^*)_{j,k-1/2}]\} \\ &= \frac{(\rho q)_{j,k-1/2}}{q_{j,k+1/2}} + \frac{1}{q_{j,k+1/2}}[\{(\rho^* q^*)_{j,k+1/2} \\ &\quad -(\rho^* q^*)_{j,k-1/2}\}].\end{aligned} \tag{14}$$

For steady supersonic flows where $(\rho^* q^*)$ is a constant everywhere, Eq. (14) reduces to

$$\tilde{\rho}_{j,k+1/2} = \rho_{j,k-1/2}\left\{\frac{q_{j,k-1/2}}{q_{j,k+1/2}}\right\}. \tag{15}$$

3) Transition Through Sonic Line ($q > q^*$ at $k+1/2$ and $q < q^*$ at $k-1/2$. Refer to Fig. 1a.) For $U > 0$,

$$\begin{aligned}\tilde{\rho}_{j,k+1/2} &= \frac{1}{q_{j,k+1/2}}\{(\rho q)_{j,k+1/2} \\ &\quad - [(\rho q - \rho^* q^*)_{j,k+1/2} - \cancelto{0}{(\rho q)^-_{j,k-1/2}}]\} \\ &= \frac{\rho^* q^*}{q_{j,k+1/2}}.\end{aligned} \tag{16}$$

4) Transition Through Shock ($q > q^*$ at $k-1/2$ and $q < q^*$ at $k+1/2$. Refer to Fig. 1b.) For $U > 0$,

$$\begin{aligned}\tilde{\rho}_{j,k+1/2} &= \frac{1}{q_{j,k+1/2}}\{(\rho q)_{j,k+1/2} \\ &\quad - [\cancelto{0}{(\rho q)^-_{j,k+1/2}} - (\rho q - \rho^* q^*)_{j,k-1/2}]\} \\ &= \rho_{j,k+1/2} + \frac{1}{q_{j,k+1/2}}\{\rho q - \rho^* q^*\}_{j,k-1/2}\end{aligned} \tag{17}$$

For steady flows where $\rho^* q^*$ is a constant, it can be shown that at a pure supersonic point (case 2 above), the

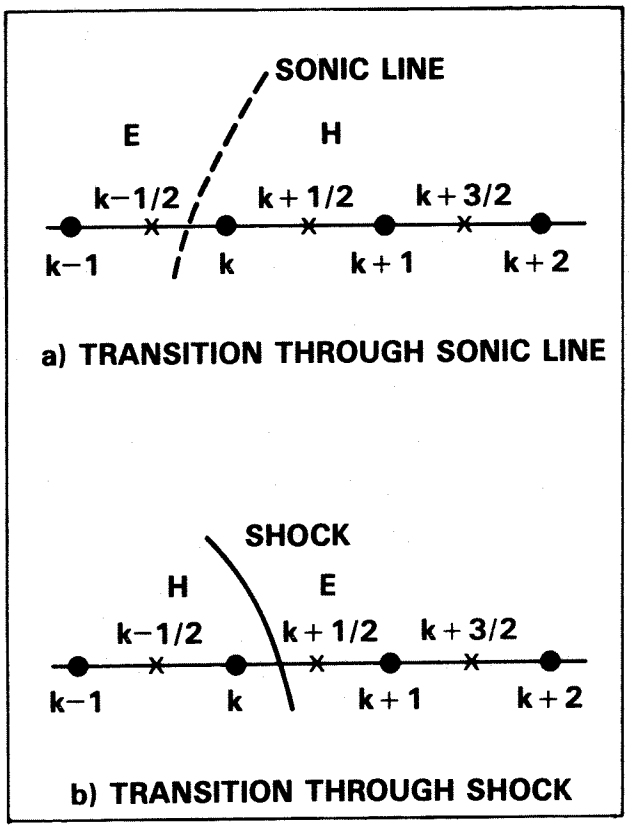

Fig. 1. Notation for flux biasing.

flux biasing procedure, Eq. (8), and the usual density biasing technique of Ref. 2, Eq. (7), are identical.

$$\frac{\partial \rho}{\partial q} = -\frac{\rho}{a^2} q \tag{18}$$

$$\frac{\partial \rho}{\partial \zeta} = \frac{\partial \rho}{\partial q}\frac{\partial q}{\partial \zeta} = -\frac{\rho}{a^2} q q_\zeta \tag{19}$$

$$\begin{aligned} \frac{\partial}{\partial \zeta}(\rho q)^- &= \frac{\partial}{\partial \zeta}(\rho q - \rho^* q^*) \\ &= \frac{\partial}{\partial \zeta}(\rho q) \text{ (for steady flows only)} \\ &= \rho_\zeta q + \rho q_\zeta \end{aligned} \tag{20}$$

Using Eq. (20)

$$\begin{aligned} \frac{\partial}{\partial \zeta}(\rho q)^- &= \rho_\zeta q \left\{1 - \frac{a^2}{q^2}\right\} \\ &= \rho_\zeta q \left\{1 - \frac{1}{M^2}\right\}. \end{aligned} \tag{21}$$

Using Eq. (21), thus, for a pure supersonic point, Eq. (8) becomes, for $U > 0$

$$\tilde{\rho}_{j,k+1/2} = \frac{1}{q_{j,k+1/2}} \left\{\rho q - \Delta\zeta \overleftarrow{\rho}_\zeta q \left(1 - \frac{1}{M^2}\right)\right\}_{j,k+1/2} \tag{22}$$

Using $\nu = \left(1 - \frac{1}{M^2}\right)$, Eq. (22) can be written as

$$\begin{aligned} \tilde{\rho}_{j,k+1/2} &= \rho_{j,k+1/2} - \nu(\rho_{j,k+1/2} - \rho_{j,k-1/2}) \\ &= (1-\nu)\rho_{j,k+1/2} + \nu\rho_{j,k-1/2}. \end{aligned} \tag{23}$$

Equation (23) is the usual density biasing technique of Holst[2]. However, while transitioning through a sonic line (case 3) or through a shock (case 4), the flux biasing procedure of Eq. (8) accurately monitors the sonic conditions ρ^* and q^*, as given by Eqs. (16) and (17).

The advantages of flux biasing over the density biasing[2] scheme are:

1. Does not require any user–specified constants (the parameter 'c' in Ref. 2) that depend on the severity of the flow.
2. Provides a monotone profile through the shock wave (for details, see Refs. 12 and 13).
3. Allows for larger Courant numbers to be taken during the calculation (by not producing undesired pressure overshoots at shocks, which could cause instability during transient calculations).
4. Provides a two point transition through a shock wave.

A detailed mathematical description of the flux biasing procedure can be found in the works of Osher[12] and Hafez[13].

E. Unsteady Wake Treatment

Figure 2 shows the schematic of a wake cut behind the trailing edge of an airfoil. This wake cut has to be properly modeled in the unsteady formulation. An expression for the jump in ϕ across the wake cut can be derived by requiring that the pressure be continuous across the cut. In the full potential framework, this results in the continuity of density. Equating the density $\rho_u = \rho_\ell$ at any point along the wake (refer to Fig. 2), one can write

$$2\Gamma_t + (U_u + U_\ell)(\phi_\zeta)_u - U_\ell \Gamma_\zeta = 0 \tag{24}$$

assuming $[V\phi_\eta] \cong 0$, where $[f]$ stands for the jump in the quantity given by $(f_u - f_\ell)$. Equation (24) is integrated from the trailing edge to the downstream boundary (along TE in Fig. 2) to obtain the Γ distribution along the wake cut. To maintain stability, the ζ derivatives in Eq. (24) are upwind differenced. For a steady flow, Eq. (24) will result in a constant value for Γ along the wake given by $\Gamma = \phi_T - \phi_{T'}$ in Fig. 2.

Beside the Γ evaluation, solution to the unsteady equation also requires information on (ϕ_η) at a wake point. Referring to Fig. 2 for notation, one can write the following using Taylor's series expansion.

$$\begin{aligned} \phi_2 &= \phi_3 - (\phi_\eta)_u + (\phi_{\eta\eta})_u/2 + \cdots \\ \phi_{\bar{2}} &= \phi_{\bar{3}} - (\phi_\eta)_\ell + (\phi_{\eta\eta})_\ell/2 + \cdots \end{aligned} \tag{25}$$

The subscripts 'u' and 'ℓ' stand for upper and lower, respectively.

For the chosen coordinate system, requiring that $(\phi_\eta)_u = -(\phi_\eta)_\ell$ and defining $\phi_2 - \phi_{\bar{2}} = \Gamma$, using Eqs. (25) one can write

$$(\phi_\eta)_u = \frac{\phi_3 - \{\phi_{\bar{3}} + \Gamma + [\phi_{\eta\eta}]/2\}}{2} \tag{26}$$

Equation (26) requires an estimate for the jump in $\phi_{\eta\eta}$ at the wake cut. This can be obtained by setting the jump in the equation to be zero at a wake point.

$$\left[\left(\frac{\rho}{J}\right)_\tau + \left(\rho\frac{U}{J}\right)_\zeta + \left(\rho\frac{V}{J}\right)_\eta\right] = 0. \tag{27}$$

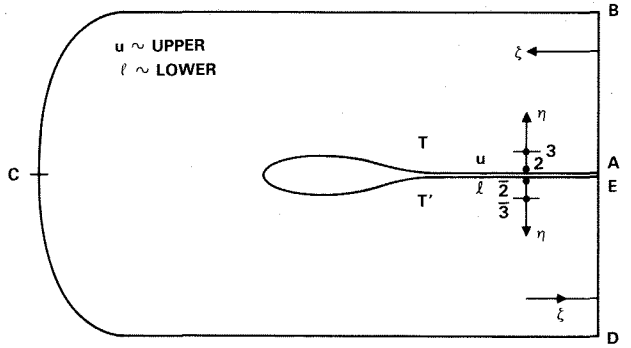

Fig. 2. Wake and outer boundary treatment.

Writing down Eq. (27) in terms of the transformation metrics and requiring that $\rho_u = \rho_\ell$, the following relationship is obtained.

$$[\phi_{\eta\eta}] = -\frac{(\rho a_{11}\Gamma_\varsigma)_\varsigma}{\rho a_{22}}. \tag{28}$$

For steady flows, the jump in $\phi_{\eta\eta}$ along the wake is zero because $\Gamma_\varsigma = 0$. For unsteady flows, to maintain accuracy, Eqs. (24)-(28) have to be employed.

F. Far Field Boundary Condition

Along the outer boundary ABCDE in Fig. 2, appropriate Riemann invariants are prescribed. The concept can be explained by considering the Cartesian form of the full potential equation cast in terms of the Riemann invariants.

$$\begin{aligned}
&\frac{\partial}{\partial t}\left(u + \frac{2}{\gamma-1}a\right) + (u+a)\frac{\partial}{\partial x}\left(u + \frac{2}{\gamma-1}a\right) = 0 \\
&\frac{\partial}{\partial t}\left(u - \frac{2}{\gamma-1}a\right) + (u-a)\frac{\partial}{\partial x}\left(u - \frac{2}{\gamma-1}a\right) = 0
\end{aligned} \tag{29}$$

Equation (29) implies that along the $(u+a)$ positive characteristics the quantity $\left(u + \frac{2}{\gamma-1}a\right)$ is invariant, and along the $(u-a)$ negative characteristics the quantity $\left(u - \frac{2}{\gamma-1}a\right)$ is invariant, known as the Riemann invariants. Usually, along the outer boundary, the Riemann invariant that corresponds to the positive characteristics with respect to the inward normal can be prescribed as a boundary condition.

For an arbitrary coordinate system (τ, ς, η), such as the one in Fig. 2, the following boundary conditions are appropriate.

$$\begin{aligned}
&\frac{U}{\sqrt{a_{11}}} + \frac{2}{\gamma-1}a = \text{constant along AB} \\
&-\frac{U}{\sqrt{a_{11}}} + \frac{2}{\gamma-1}a = \text{constant along ED} \\
&-\frac{V}{\sqrt{a_{22}}} + \frac{2}{\gamma-1}a = \text{constant along BCD}
\end{aligned} \tag{30}$$

Equation (30) is nonlinear in nature. Hence, to implement the Riemann invariant boundary condition, a linearization technique similar to Eq. (3) is employed. For example, equating the right hand side of Eq. (30) to the freestream value, along BCD one can write

$$\begin{aligned}
&-\frac{\left(a_{12}\frac{\partial}{\partial\varsigma} + a_{22}\frac{\partial}{\partial\eta}\right)^n \Delta\phi}{\sqrt{a_{22}}} \\
&-\frac{1}{a^n}\left(\frac{\partial}{\partial\tau} + U\frac{\partial}{\partial\varsigma} + V\frac{\partial}{\partial\eta}\right)^n \Delta\phi
\end{aligned} \tag{31}$$

$$= \left(-\frac{V}{\sqrt{a_{22}}} + \frac{2}{\gamma-1}a\right)_{\text{freestream}} - \left(-\frac{V}{\sqrt{a_{22}}} + \frac{2}{\gamma-1}a\right)^n$$

The finite differenced form of Eq. (31) will provide an estimate for $(\Delta\phi)$ along the outer boundary. Use of the Riemann invariant boundary conditions is better than prescribing ϕ_∞ from the compressible vortex solution, and will serve as a nonreflecting boundary condition.

G. Relaxation and Approximate Factorization Schemes

When all the terms of Eq. (1) are put together, it will be in terms of the unknown $\Delta\phi$. It can be written as

$$F(\Delta\phi) + R(\phi^n, \phi^{n-1}, \cdots) = 0 \quad , \quad \Delta\phi = \phi^{n+1} - \phi^n. \tag{32}$$

The Newton iterative procedure for solving Eq. (32) becomes

$$\frac{\partial F}{\partial \Delta\phi}(\Delta\phi^{n+1} - \Delta\phi^i) = -R(\phi^n, \phi^{n-1}, \cdots) - F(\Delta\phi^i) \tag{33}$$

The off-diagonal elements of $\frac{\partial F}{\partial \Delta\phi}$, which cannot be accommodated within the tridiagonal setup of SLOR, can be set to zero. In Eq. (33), $\Delta\phi^i$ represents the intermediate iterative value of $\Delta\phi$. For steady state problems, $\Delta\phi^i$ can be set to $\Delta\phi^n$. If all the off-diagonal terms of $\frac{\partial F}{\partial \Delta\phi}$ are set to zero, then the relaxation process becomes the point Jacobi iteration. Results based on the relaxation procedure of Eq. (32) are presented in this paper.

Another procedure to solve Eq. (32) is the approximate factorization technique. This can be written as

$$L_\varsigma L_\eta \Delta\phi = R \tag{34}$$

where

$$L_\varsigma = \left[1 + \Delta\tau_1 U\frac{\partial}{\partial\varsigma} + \frac{\alpha}{\beta}\frac{\partial}{\partial\varsigma}\frac{\tilde{\rho}^*}{J}a_{11}\frac{\partial}{\partial\varsigma}\right]$$

$$L_\eta = \left[1 + \Delta\tau_1 V\frac{\partial}{\partial\eta} + \frac{\alpha}{\beta}\frac{\partial}{\partial\eta}\frac{\tilde{\rho}^*}{J}a_{22}\frac{\partial}{\partial\eta}\right]$$

$$\beta = -\left(\frac{\rho^n}{J^{n+1}(a^n\Delta\tau_1)^2}\right)_{j,k}$$

$$\alpha = (1-\theta) + \theta\left[\{a_1 - b_1(\Delta\tau_1 + \Delta\tau_2)/\Delta\tau_1\}/\{a_1 - b_1\}\right]$$

Equation (34) is solved at the $(n+1)$ plane in two steps.

$$L_\varsigma\overline{\Delta\phi} = R \quad , \quad \text{Step 1}$$

$$L_\eta\Delta\phi = \overline{\Delta\phi} \quad , \quad \text{Step 2}$$

$$\phi^{n+1}_{j,k} = \phi^n_{j,k} + \Delta\phi_{j,k}$$

Both L_ς and L_η result in tridiagonal matrices.

H. Body Boundary Condition

For inviscid flows, the surface flow tangency condition dictates that the contravariant velocity, V, be zero at the body. Implementation of the condition, $V = 0$, in the L_η operator is a crucial step in achieving a true implicit scheme. Usually, the boundary condition $V = 0$ is set only in the right hand side term R, and a careless or no boundary condition treatment is imposed in the left hand side L_η operator[2]. In the present method, the condition $V = 0$ is imposed on both sides of Eq. (34). Let $j = J$ denote the body point. Then,

$$V = (a_{12}\phi_\varsigma + a_{22}\phi_\eta)_{J,k} = 0 \tag{35}$$

or

$$(\phi_\eta)_{J,k} = -\left(\frac{a_{12}}{a_{22}}\phi_\zeta\right)_{J,k}. \tag{36}$$

Using Eqs. (35) and (36), and the relationship

$$\left(\rho\frac{V}{J}\right)_{J-1/2} = -\left(\rho\frac{V}{J}\right)_{J+1/2}, \tag{37}$$

the L_ζ and the L_η operators in Eq. (34) can be modified to the form, for a body point J,

$$\tilde{L}_\zeta \tilde{L}_\eta \Delta\phi = \tilde{R} \tag{38}$$

where

$$\tilde{L}_\zeta = \left[1 + \Delta\tau_1 U\frac{\partial}{\partial\zeta} + \frac{\alpha}{\beta}\frac{\partial}{\partial\zeta}\frac{\tilde{\rho}}{J}\left(a_{11} - \frac{a_{12}^2}{a_{22}}\right)\frac{\partial}{\partial\zeta}\right]$$

$$\tilde{L}_\eta = \left[1 + \frac{2}{\Delta\eta}\frac{\alpha}{\beta}\left(\frac{\tilde{\rho}}{J}a_{22}\frac{\partial}{\partial\zeta}\right)_{J+1/2}\right].$$

In Eq. (38), the boundary condition is split between the two operators, $\tilde{L}_\zeta$ and $\tilde{L}_\eta$. Even for nonorthogonal mesh at the body ($a_{12} \neq 0$), the boundary condition is set implicitly. This allows for large time steps, or Courant numbers, to be taken during the calculation.

III. Results

Computer codes based on both the relaxation method (Eq. (33)) and the approximate factorization method (Eq. (34)) have been constructed for two–dimensional and axisymmetric problems. The grid around the geometry can be either a C–type (Fig. 2) or an O–type. At present, the relaxation method is somewhat slower (at least 50%) in convergence than the approximate factorization code. However, the future implementation of multigrid techniques[17] and implicit relaxation concepts[14] to the present relaxation code can make it competitive to approximate factorization methods in three–dimensional applications, where the approximate factorization methods with triple factorization can be less flexible to handle complex geometries[14].

The unsteady code has been applied, at present, only to steady state problems. Calculations involving unsteady motions such as plunge, pitch, and oscillating flaps are currently in progress. For steady state problems, the time step $\Delta\tau_1$ appearing in Eq. (34) is computed from a prescribed Courant number, usually set much greater than one (~ 50).

Figure 3 shows the result for a flow over a cylinder at $M_\infty = 0.4$. The flow is barely critical, and a comparison with an efficient Euler code[14] is excellent. Figures 4 and 5 show results for supersonic flows over a sphere at low Mach numbers of 1.08 and 1.4. The density distribution for these cases are compared with benchmark Euler calculations[15]. The present full potential code required approximately 80 time steps to converge (residual $< 10^{-5}$). It is worth noting at this point that the Euler code of Ref. 15 requires in excess of 20,000 iterations to perform the low Mach number calculation of 1.08.

Figure 6 shows the pressure distribution obtained over the NACA 0012 airfoil at $M_\infty = 0.8$ and $\alpha = 0°$ with

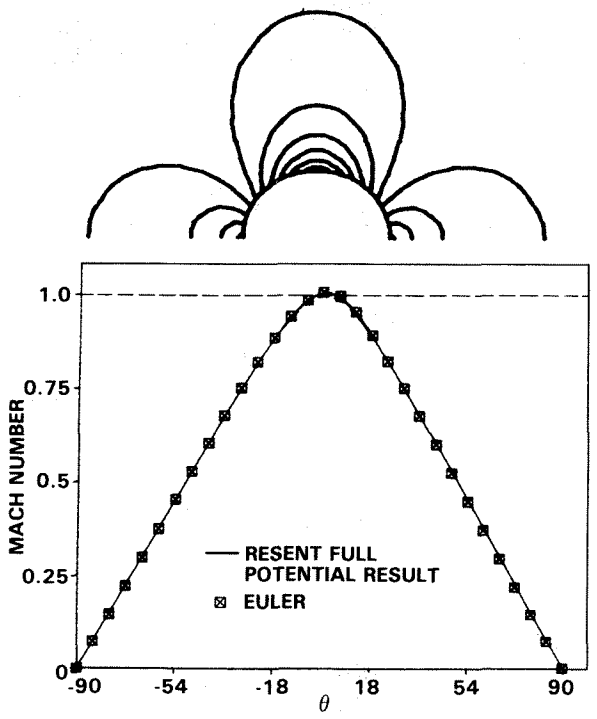

Fig. 3. Mach number distribution for cylinder flow at $M_\infty = 0.4$.

a grid of 84 points around the airfoil and 18 in the η–direction. The comparison with an Euler code[14] is good. Figure 7 shows the results for $M_\infty = 0.75$ and $\alpha = 2°$ over the same airfoil. Even with a crude grid, the formation of a strong shock without any overshoots is made possible by the use of flux biasing concepts. Calculations of this type require no user–specified "constants" to increase or decrease the amount of dissipation. Depending on the strength of the shock, the flux biasing automatically chooses the right amount of dissipation, since it is based on sonic reference conditions. The perfect matching of pressure contours across the wake cut (Fig. 7) illustrates the correctness of the unsteady wake model described in this paper. Figure 8 shows some difficult cases with fishtail shocks.

The unsteady code can also be effectively used to generate the blunt body solution, the outflow of which is to be prescribed as an initial data plane for a full potential supersonic marching code[6]. Figure 9 shows the schematic of such a hybrid calculation. The flow over the entire Shuttle Orbiter with a blunt nose has been simulated at $M_\infty = 1.4$ and $\alpha = 0°$. The results of Fig. 5 were used as a starting solution for the marching calculation[16]. The nose region geometry and the pressure distribution along the leeside symmetry of the Orbiter are shown in Figs. 10 and 11.

Simulation of unsteady phenomena, such as flutter and control surface oscillations will be presented in the future.

IV. Conclusions

A computational treatment for the unsteady full potential equation is presented. The method employs a local time linearization, flux biasing concepts for generation of

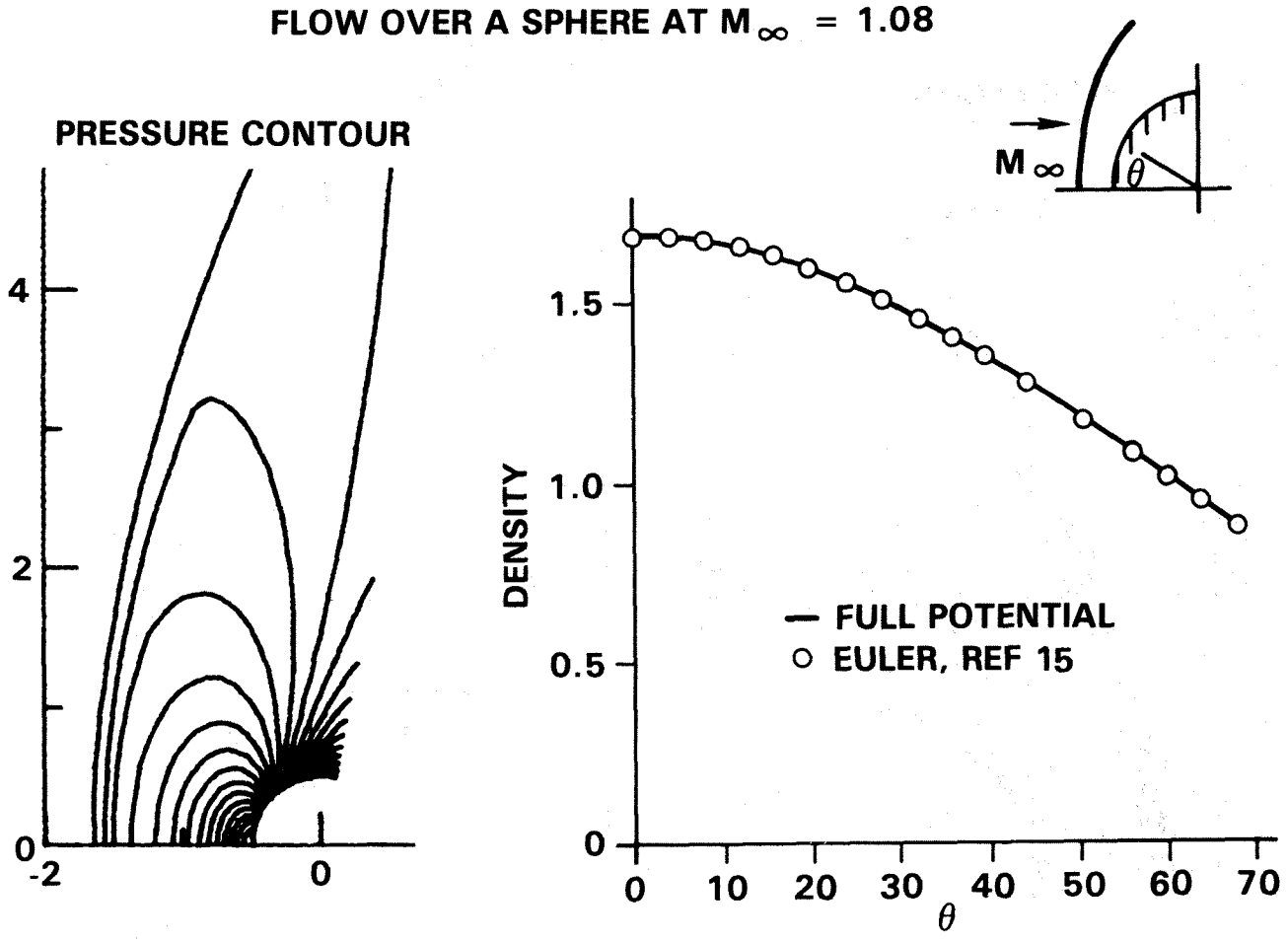

Fig. 4. Density distribution and Mach number contours for flow over a sphere at $M_{\infty} = 1.08$.

artificial viscosity, unsteady wake treatment, outer boundary conditions based on the Riemann invariants, and relaxation and approximate factorization algorithms. Use of the code for problems with steady state solution has been very effective and computationally fast. Extensions of this work to simulate unsteady phenomena such as flutter, and to three dimensions to treat wings, and wing-body combinations, are currently in progress.

V. Acknowledgement

The authors express their thanks to Prof. Osher of U.C.L.A., and Drs. Chakravarthy and Szema of Rockwell for many valuable discussions. This work was partially funded by NASA-Langley Research Center under Contract NAS1-15820.

VI. References

1. Jameson, A., "Transonic Potential Flow Calculations using Conservation Form," AIAA 2nd Computational Fluid Dynamic Conference Proceedings, 1975, pp. 148–155.
2. Holst, T.L., "Fast, Conservative Algorithm for Solving the Transonic Full Potential Equation," AIAA Journal, Vol. 18, No. 12, December 1980, pp 1431–1439.
3. Siclari, M.J., "Computation of Nonlinear Supersonic Potential Flow over Three-Dimensional Surfaces," AIAA Paper No. 82-0167, presented at the AIAA 20th Aerospace Sciences Meeting, Orlando, Florida, January 1982.
4. Shankar, V., "A Conservative Full Potential, Implicit, Marching Scheme for Supersonic Flows," AIAA Journal, Vol. 20, No. 11, November 1982, pp. 1508–1514.
5. Shankar, V. and Osher, S., "An Efficient Full Potential Implicit Method Based on Characteristics for Analysis of Supersonic Flows," AIAA Paper No. 82-0974, June 1982; AIAA Journal, Vol. 21, No. 9, p. 1262, September 1983.
6. Shankar, V., Szema, K.-Y., and Osher, S., "A Conservative Type-Dependent Full Potential Method for the Treatment of Supersonic Flows with Embedded Subsonic Regions," AIAA Paper No. 83-1887; to appear in the AIAA Journal, November 1984.
7. Chipman, R. and Jameson, A., "An Alternating Direction Implicit Algorithm for Unsteady Potential Flow," presented at the AIAA 19th Aerospace Sciences Meeting, January 1981.

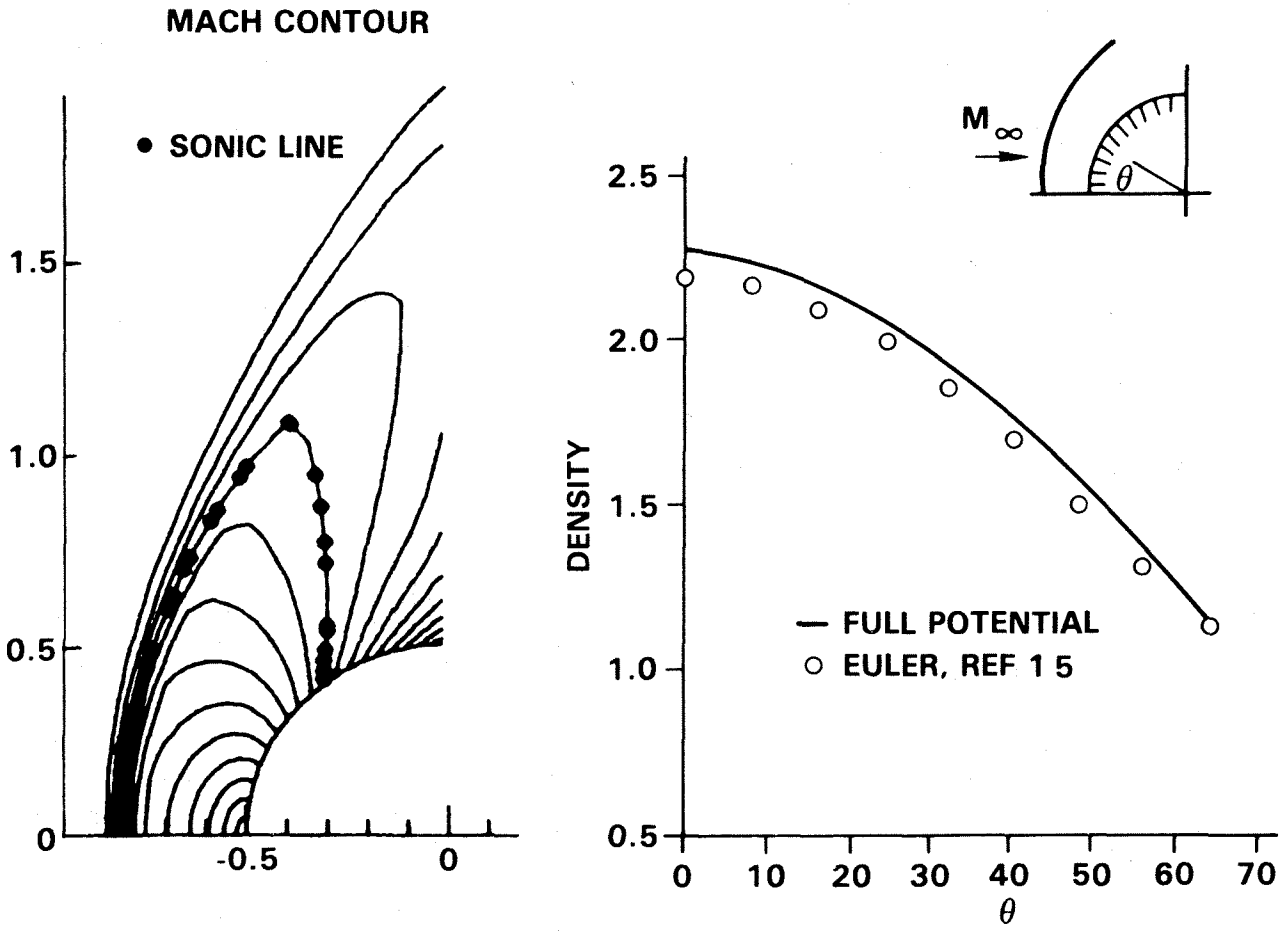

Fig. 5. Density distribution and Mach number contours for flow over a sphere at $M_\infty = 1.4$.

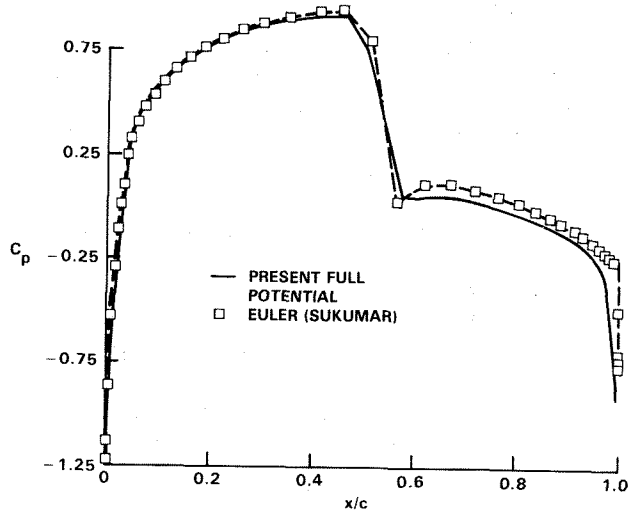

Fig. 6. Flow over NACA 0012, $M_\infty = 0.8$, $\alpha = 0°$.

8. Goorjian, P.M., "Computations of Unsteady Transonic Flow Governed by the Conservative Full Potential Equation using an Alternating Direction Implicit Algorithm," NASA CR-152274, June 1979.
9. Sankar, N.L. and Tassa, Y., "An Algorithm for Unsteady Transonic Potential Flow Past Airfoils," paper presented at the 7th International Conference on Numerical Methods in Fluid Dynamics, June 1980.
10. Steger, J. and Caradonna, F., "A Conservative Implicit Finite Difference Algorithm for the Unsteady Transonic Full Potential Equation," AIAA Paper No. 80-1368, presented at the 13th Fluid and Plasma Dynamics Conference, July 1980.
11. Malone, J.B. and Sankar, N.L., "Numerical Simulation of 2-D Unsteady Transonic Flows using the Full Potential Equation," AIAA Paper No. 83-0233.
12. Osher, S., "Scheme Design for Transonic Unsteady Aerodynamics Based on Riemann Solvers and the Entropy Condition," Transonic Unsteady Aerodynamics and Aeroelasticity Workshop, NASA-Langley Research Center, June 1983.

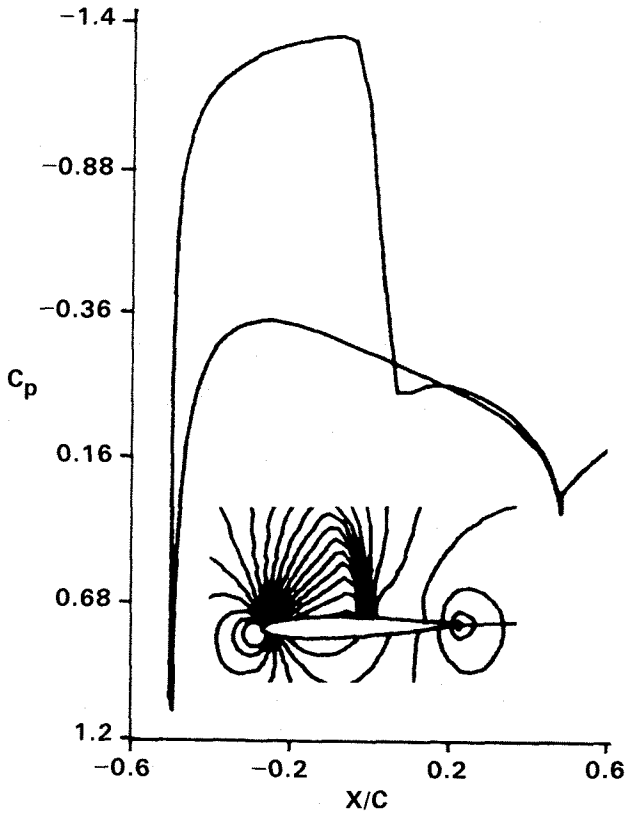

Fig. 7. Flow over NACA 0012, $M_\infty = 0.75$, $\alpha = 2°$.

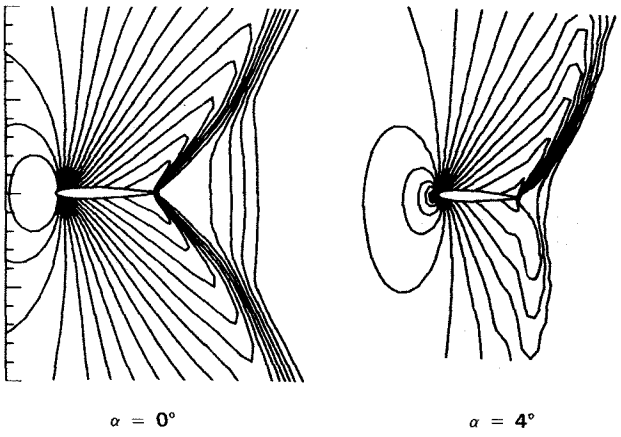

Fig. 8. Mach number contours for NACA 0012, $M_\infty = 0.98$.

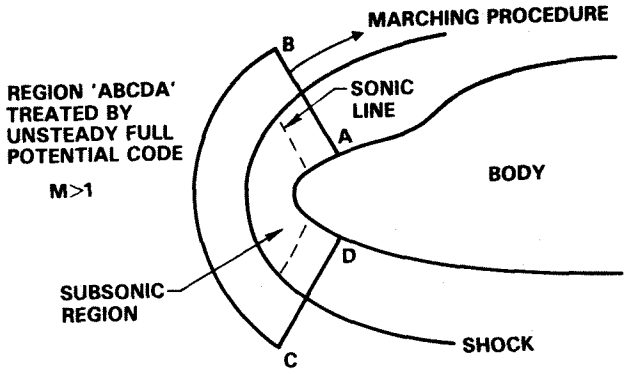

Fig.9. Blunt body starting solution for a marching code.

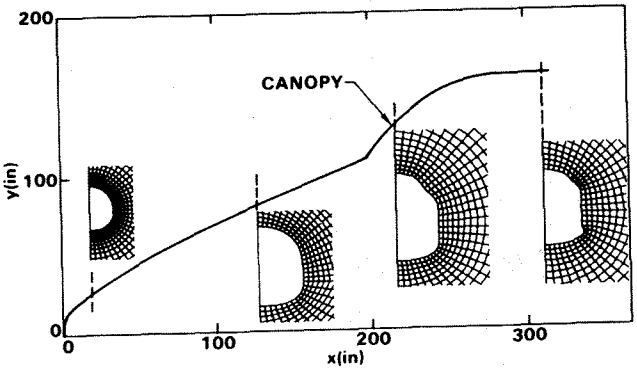

Fig. 10. Nose region geometry of Shuttle Orbiter.

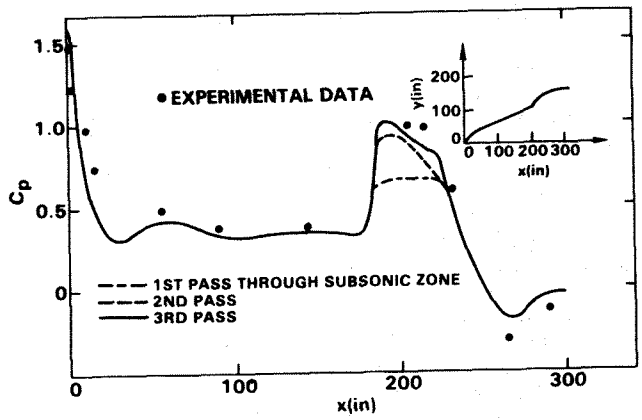

Fig. 11. Hybrid unsteady blunt body/supersonic marching calculation for the Orbiter at $M_\infty = 1.4$, $\alpha = 0°$.

13. Hafez, M., "Entropy Inequality for Transonic Flows," Transonic Unsteady Aerodynamics and Aeroelasticity Workshop, NASA–Langley Research Center, June 1983.

14. Chakravarthy, Sukumar, "Implicit Upwind Schemes without Approximate Factorization," AIAA Paper No. 84–0165.

15. Salas, M.D., "Flow Properties for a Spherical Body at Low Supersonic Speeds," Symposium on Computers in Aerodynamics, 25th Anniversary of Aerodynamics Labs, PINY, Farmingdale, NY, June 1979.

16. Szema, K.–Y. and Shankar, V., "Nonlinear Computation of Wing–Body–Vertical Tail–Wake Flows at Low Supersonic Speeds," AIAA Paper No. 84–0427.

17. South, Jr., J.C. and Brandt, A., "Application of a Multi–Level Grid Method to Transonic Flow Calculations," ICASE Report 76–8, NASA, 1976.